Effects of NH_3 and N_2 additions to hot filament activated CH_4/H_2 gas mixtures

James A. Smith, Jonathan B. Wills, Helen S. Moores, Andrew J. Orr-Ewing, and Michael N. R. Ashfold[a)]
School of Chemistry, University of Bristol, Bristol BS8 1TS, United Kingdom

Yuri A. Mankelevich and Nikolay V. Suetin
Nuclear Physics Institute, Moscow State University, 119899 Moscow, Russia

(Received 1 October 2001; accepted for publication 5 April 2002)

Resonance enhanced multiphoton ionization and cavity ring down spectroscopies have been used to provide spatially resolved measurements of relative H atom and CH_3 radical number densities, and NH column densities, in a hot filament (HF) reactor designed for diamond chemical vapor deposition and here operating with a 1% $CH_4/n/H_2$ gas mixture—where n represents defined additions of N_2 or NH_3. Three-dimensional modeling of the H/C/N chemistry prevailing in such HF activated gas mixtures allows the relative number density measurements to be placed on an absolute scale. Experiment and theory both indicate that N_2 is largely unreactive under the prevailing experimental conditions, but NH_3 additions are shown to have a major effect on the gas phase chemistry and composition. Specifically, NH_3 additions introduce an additional series of ''H-shift'' reactions of the form $NH_x + H \rightleftharpoons NH_{x-1} + H_2$ which result in the formation of N atoms with calculated steady state number densities $>10^{13}$ cm^{-3} in the case of 1% NH_3 additions in the hotter regions of the reactor. These react, irreversibly, with C_1 hydrocarbon species forming HCN products, thereby reducing the concentration of free hydrocarbon species (notably CH_3) available to participate in diamond growth. The deduced reduction in CH_3 number density due to competing gas phase chemistry is shown to be compounded by NH_3 induced modifications to the hot filament surface, which reduce its efficiency as a catalyst for H_2 dissociation, thus lowering the steady state gas phase H atom concentrations and the extent and efficiency of all subsequent gas phase transformations. © *2002 American Institute of Physics.* [DOI: 10.1063/1.1481961]

I. INTRODUCTION

Addition of trace (ppm) amounts of nitrogen (as N_2 or in the form of an N containing gas like NH_3) to the typical hydrocarbon/H_2 gas mixtures used for diamond chemical vapor deposition (CVD) in both hot filament (HF) and microwave (MW) reactors can lead to enhanced deposition rates, affect the growth habit, cause macrostep bunching, lead to (modest) nitrogen incorporation in substitutional lattice sites, and thereby affect the electrical and field emission properties of the resulting films.[1–20] May and co-workers[21–23] investigated diamond CVD in both HF and MW reactors using $CH_4/NH_3/H_2$, CH_3NH_2/H_2, and HCN/H_2 gas mixtures. The aims of their studies were two fold; namely, to see whether use of such alternative N containing precursors provided a route to enhanced nitrogen incorporation in the as-grown diamond film, and to unravel aspects of the chemistry prevailing in H/C/N containing gas mixtures using *in situ* molecular-beam mass spectrometry (MBMS) to sample the gas phase composition in the vicinity of the HF. Diamond CVD was observed from $CH_4/NH_3/H_2$ feedstock gas mixtures, provided the input gas ratio $[CH_4]:[NH_3] \geqslant 1$, but the addition of NH_3 was found to reduce deposition rates relative to those found for a simple CH_4/H_2 gas mixture. CH_3NH_2/H_2 and HCN/H_2 gas mixtures were also shown to yield CVD diamond, with (low) efficiencies comparable to that found using 1:1 mixtures of CH_4 and NH_3 in H_2.[21] Such findings are explicable given the MBMS measurements, which showed substantial conversion of the input carbon to HCN, the thermodynamically favored product, at the relevant process temperatures.[22] Thus, it was proposed that HCN acts as a sink for carbon that might otherwise have participated in diamond growth.

The combined program of experiment and modeling presented here aims to provide a more detailed interpretation of the effects of controlled additions of nitrogen (in the form of N_2 and NH_3) to HF activated CH_4/H_2 process gas mixtures at mole fractions appropriate for, and well beyond those used in, successful diamond deposition. As such, the study provides a rather stringent test of the current understanding of H/C/N gas phase chemistry, over a wide temperature range. The experimental work involves use of resonance enhanced multiphoton ionization (REMPI) spectroscopy to provide spatially resolved *in situ* measurements of H atom and CH_3 radical number densities, and cavity ring down spectroscopy (CRDS)[24–26] to provide similar measurements of NH radical column densities, as a function of process conditions (e.g., feedstock gas mixing ratio and the temperature, T_{fil}, of the Ta filament). The REMPI measurements serve to extend recent investigations of diamond CVD when using CH_4/H_2

a)Author to whom all correspondence should be addressed; electronic mail: mike.ashfold@bris.ac.uk

and C_2H_2/H_2 gas mixtures in the same HF-CVD reactor.[27–29] These experimental results are compared with the output of an existing three-dimensional (3D) model,[30] tailored specifically to this HF-CVD reactor. The model comprises three blocks, which describe (i) activation of the reactive mixture (i.e., gas heating and catalytic H atom production at the filament surface), (ii) gas-phase processes (heat and mass transfer and chemical kinetics), and (iii) gas-surface processes at the substrate. The final subroutine is not required in the present work, since the experiments to be modeled were all performed with no substrate in place. The gas-phase chemistry and thermochemical input is taken from the GRI-Mech 3.0 detailed reaction mechanism for C/H/N/O gas mixtures,[31] supplemented by one additional reaction allowing destruction of the species H_2CN, but with all reaction steps and species involving O atoms removed. As in previous studies,[30,32,33] the conservation equations for mass, momentum, energy, and species concentrations, together with appropriate initial and boundary conditions, thermal, and caloric equations of state, are each integrated numerically until steady-state conditions are attained, thereby yielding spatial distributions of the gas temperature, T_{gas}, the flow field, and the various species number densities and mole fractions. Comparisons between the experimental and model results serve to illustrate the very different reactivities of N_2 and NH_3 in the present HF activated 1% CH_4/H_2 gas mixtures, and reveal details both of the gas-phase chemistry prevailing when using $CH_4/NH_3/H_2$ process gas mixtures, and the reduction in H atom production rate on the surface of the HF when NH_3 is added to the process gas mixture.

II. EXPERIMENT

Details of the HF-CVD reactor, and the REMPI detection schemes used for spatially resolved measurements of H atom and CH_3 radical number densities have been presented elsewhere[27–29,33] and are here summarized only very briefly. CRDS measurements in this reactor will be described in somewhat greater detail.

The reactor is an evacuable stainless steel six-way cross equipped with quartz windows to allow passage of the probe laser beam and, along an orthogonal axis, viewing of the HF with a two color optical pyrometer (Land Infrared). The HF (250 μm diameter Ta wire, seven turns, ~3 mm coil diameter) is attached to a cradle suspended below a linear transfer mechanism mounted on the top flange of the reactor; this allows the HF to be translated vertically, by ⩽25 mm, relative to the fixed laser focus and the tip of a negatively biased Pt probe wire used for ion collection. Power is supplied from a dc power supply via feedthroughs to one side of the HF; its other end is grounded. The H_2, CH_4, NH_3, and/or N_2 feedstock gases are metered through separate mass flow controllers, premixed in a manifold, and enter the reactor through a port located above the cradle assembly, so as to maintain an overall flow rate of 100 sccm and total pressure of 20 Torr. H atoms and CH_3 radicals are both detected by $2+1$ REMPI using UV excitation wavelengths of, respectively, 243.1 nm and ~333 nm, both of which are produced by frequency doubling the output of a Nd–YAG pumped tunable dye laser

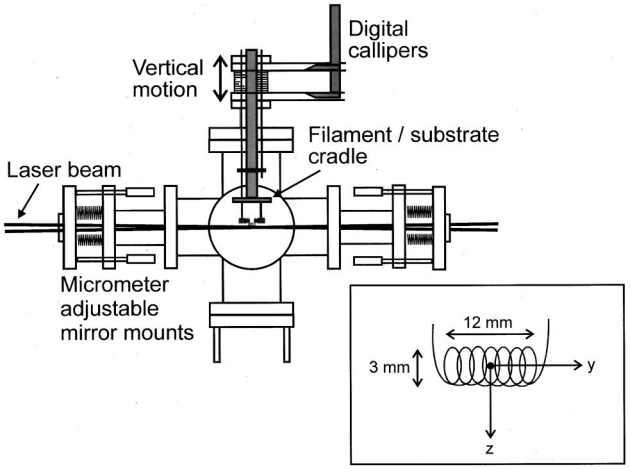

FIG. 1. Schematic of the HF-CVD reactor configured for CRDS measurements. The inset at the bottom right-hand side shows an enlarged schematic of the filament region and coordinate system used in the numerical modelling. In the model calculation, gas enters and exits at $z=-26$ mm and $+26$ mm, respectively. The filament consists of seven loops (3 mm diameter) of Ta wire, and is of overall length 12 mm (along y).

(Spectra-Physics DCR 2A plus PDL 3). The transient ion current resulting from REMPI in the focal region within the reactor, and the signal from the photodiode used to monitor the UV light intensity (to allow power normalization of the measured REMPI signals), are passed to a digital oscilloscope and then to a personal computer (PC) for storage and subsequent analysis.

CRDS measurements involved slight adaptation of the reactor to allow for mounting of the ring down mirrors, but otherwise similar operating conditions. The Pt probe wire used in the REMPI measurements was removed from the reactor and, as shown in Fig. 1, two of the flange mounted windows were replaced with ''mirror mount'' flanges which were designed and fabricated in house. Each consists of two stainless steel plates separated by edge welded bellows and held apart by four micrometer adjustable supports. The two high reflectivity mirrors [Virgo Lightning Optical Corporation, $R\sim99.7\%$ at ~336 nm, the wavelength required for detection of NH(X) radicals via their $A\,^3\Pi-X\,^3\Sigma^-$ transition] are mounted within the vacuum by attachment to the outer plates, and aligned parallel using the micrometers, thus forming an optical cavity of length $L=63$ cm. Frequency doubled dye laser radiation at ~336 nm is coupled into the cavity through the rear of one of the mirrors and its subsequent ring down (with a $1/e$ time constant, $\tau\sim590$ ns when the reactor is fully evacuated) detected by a photomultiplier tube (PMT) mounted external to the other mirror. Absolute frequency calibration is assured by directing a small part of the fundamental dye laser radiation into a wavemeter (Coherent-Ealing, ''Wavemaster''). The PMT signal is recorded by an eight-bit digital oscilloscope (LeCroy 9361) and the ring down trace passed to a PC through a general purpose interface bus connection. Each individual ring down trace is analyzed by linear fitting to its natural logarithm. This gives a ring down rate coefficient (k) and, as the laser frequency is scanned across a spectroscopic transition, the

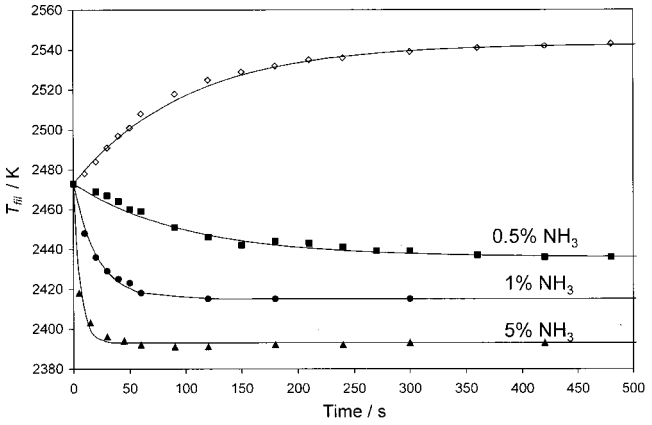

FIG. 2. Variation in the measured T_{fil} as a function of time after introducing 0.5% NH_3 (■), 1% NH_3 (●) and 5% NH_3 (▲) to a 1% CH_4 in H_2 gas mixture. The solid lines are best fits to these data sets in terms of Eq. (1) with $\tau = 100$ s (0.5% NH_3), 21 s (1% NH_3), and 6 s (5% NH_3). Also shown is one additional plot illustrating the time dependent recovery of T_{fil} upon curtailing a flow 2% NH_3 (◇) together with its best fit in terms of Eq. (1) and a time constant $\tau = 100$ s.

difference, Δk, in the ring down rate coefficient ''on'' and ''off'' the resonance is proportional to the absorption coefficient, α:

$$\alpha = \frac{L\Delta k}{c\ell}. \tag{1}$$

ℓ in Eq. (1) is the length of the column of gas containing NH radicals, c is the speed of light, and

$$\alpha = \sigma_{abs}[\mathrm{NH}], \tag{2}$$

where σ_{abs} is the NH absorption cross section. The key experimental measurable is the absorbance per pass, $\alpha\ell$, which is derived directly from determination of the ring down rates [from Eq. (1)] without any assumptions of absorption pathlength or local temperature along the column.

III. RESULTS AND DISCUSSION

A. Modifications of the hot filament upon addition of nitrogen containing gases

Addition of NH_3 to a 1% CH_4/H_2 gas mixture activated by a Ta HF was observed to cause a reduction in the T_{fil} value recorded by the two color optical pyrometer. No such decrease was observed upon addition of a corresponding flow rate of N_2. Figure 2 illustrates these effects, via plots of T_{fil} versus time after the introduction of various partial pressures of NH_3 to an established 1% CH_4 in H_2 gas mixture. In each case, the filament had been run for >6 h with the CH_4/H_2 gas mixture prior to the NH_3 (or N_2) addition, and the power supplied to the filament was held constant. Clearly, both the rate and the extent of the temperature drop, ΔT_{fil} (the difference between T_{fil} measured prior to any NH_3 addition and the asymptotic value found at long time, $t = \infty$) increase with increasing NH_3 fraction. The T_{fil} versus t trends measured for the various NH_3 partial pressures are each well described by

$$T_{fil}(t) - T_{fil}(t=\infty) = \Delta T_{fil}\exp(-t/\tau), \tag{3}$$

with a time constant, τ, that decreases as the NH_3 fraction in the input gas feed is increased. Figure 2 also provides one illustration, for the specific case of a filament conditioned with a 1% CH_4/2% NH_3/H_2 gas mixture at a maintained temperature of 2473 K, of the way T_{fil} *increases* (with a time constant that is independent of the actual NH_3 flow rate) when the NH_3 flow is shut off. Prior to any NH_3 addition, we envisage the HF as being ''carburized,'' i.e., to be mainly tantalum carbide, with a surface that is partially shrouded by a coating of graphitic carbon. Given knowledge of the input power supplied to the HF [$P_{input} = 87$ W for $T_{fil}(t=0) = 2473$ K in Fig. 2] and estimates of the power expended on H_2 dissociation ($P_{diss} \sim 8$ W) and conductive losses ($P_{cond} \sim 10.7$ W) from the 3D modeling, we can estimate the power radiated by the HF ($P_{rad} \sim 68$ W). This, in turn, allows estimation of the mean emissivity, ε, of the HF via the relationship

$$P_{rad} = \varepsilon\sigma S T_{fil}^4, \tag{4}$$

where σ is the Stefan–Boltzmann constant and S is the surface area of the HF (0.63 cm^2). The emissivities so derived, $\varepsilon \sim 0.52$ and ~ 0.61 for the addition of, respectively, 0% and 1% NH_3, lie between the literature values for the emissivity of polished TaC ($\varepsilon \sim 0.3$)[34] and graphite ($\varepsilon \sim 0.9$)[35] at $T \sim 2500$ K implying that, under these conditions, ~50% of the HF surface has a graphitic overcoat.

The observed time dependence of T_{fil} upon addition of NH_3 can be understood in terms of dynamic competition between the adsorption of N and C containing entities onto, and desorption and/or etching from, the HF surface. Two limiting mechanisms merit consideration. One assumes that, when both N and C containing species are present, the former are adsorbed preferentially leading to a surface that is preferentially ''N terminated.'' The other assumes that NH_3 addition causes a reduction in the concentration of C containing species in the gas phase near the HF, and thus to the extent of carburisation of the HF. These are considered in turn.

The reported emissivity of polished TaN ($\varepsilon \sim 0.6$ at ~2600 K)[34] is significantly higher than that of polished TaC. Assuming this trend to be applicable also to the (unpolished) surface of a Ta HF in the presence of CH_4/H_2 and $CH_4/NH_3/H_2$ gas mixtures, it is tempting to suggest that any N termination (being more analogous to TaN) will affect the energy balance of the HF and cause a progressive reduction both in T_{fil}—consistent with the present observations—and, as shown below, in Q, the net rate of H atom production per unit area of the HF surface. In this picture, the observed time dependence of T_{fil} [Eq. (3)] can be rationalized by a simplified adsorption–desorption/etching kinetic scheme in which accommodation of a nitrogen containing gas phase species A on a surface site S* leads to N termination, i.e.,

$$\mathrm{A} + \mathrm{S}^* \rightleftharpoons \mathrm{SN}. \tag{5}$$

The time dependence of θ, the N surface coverage, will then follow

$$\theta = \frac{k_5[A]}{k_5[A]+k_{-5}}(1-\exp[-(k_5[A]+k_{-5})t], \tag{6}$$

where $[A]$ is the number density of N containing species near the HF surface and k_5 and k_{-5} are, respectively, the forward and reverse reaction rate coefficients. Fitting the observed time evolution of T_{fil} upon addition of 1% and 5% NH_3 to a 1% CH_4 in H_2 gas mixture with $T_{fil}(t=0)\sim 2473$ K (Fig. 2), yields values of $k_{-5}\sim 0.01\ s^{-1}$ and $k_5[A]=0.038\ s^{-1}$ and $0.157\ s^{-1}$, respectively. Equation (6) also successfully reproduces the observed recovery of T_{fil} when the NH_3 flow is shut off (and $[A]\rightarrow 0$).

We now turn to consider the possible alternative explanation for the observed fall in T_{fil} upon NH_3 addition. In developing this argument, we first note that falls in T_{fil} have been reported previously in the case of carburised Ta filaments operating with CH_4/H_2 gas mixtures at high temperatures and constant P_{input} when the hydrocarbon content is suddenly reduced.[36,37] Such observations might appear to run counter to the previous discussion, since a reduction in the number density of gas-phase carbon might be expected to diminish the extent of any graphitic overcoat on the HF surface, thereby reducing the overall emissivity and causing T_{fil} to rise. The apparent contradiction has been explained by recognizing that the graphitic overcoat is much less efficient than a "clean" TaC surface at catalyzing H_2 dissociation.[36–38] The observed drop in T_{fil} in such experiments is then attributable to the increased fraction of P_{input} expended on surface catalyzed H_2 dissociation. As shown previously,[21,22] and in more detail later in this article, one effect of NH_3 addition in the present experiments is to convert CH_4 molecules into HCN in the hotter regions of the gas. HCN is a stable molecule in this environment, and thus acts as a "sink" for gas phase carbon near the HF. Adding NH_3 to a CH_4/H_2 gas mixture thus has a similar effect to simply reducing the CH_4 input flow rate; both lead to a reduced number density of gas phase carbon available for formation of any graphitic layer on the HF surface. This would cause an increase in the number of active sites S* capable of catalysing H_2 dissociation, and an increase in P_{diss}, which would be reflected in a fall in P_{rad} and thus in the observed T_{fil}. We note, however, that the earlier experiments involved much higher T_{fil} values (and thus a very different partitioning of P_{input}) than the present work. At $T_{fil}>2800$ K—the filament temperatures used in the earlier studies[36,37]—P_{diss} and P_{rad} are of comparable magnitude, so any increase in P_{diss} as a result of changes in the relative surface coverage by TaC and by graphite would have a very noticeable effect on P_{rad} and thus T_{fil}. The present studies employ much lower T_{fil} values where P_{diss} is estimated to account for less than 10% of P_{input}. Given such modest estimates of P_{diss}, it seems unlikely that an explanation based solely on reductions of gas phase C near the HF surface could explain T_{fil} reductions of the magnitudes shown in Fig. 2.

B. Gas phase H atom and CH_3 radical number densities as a function of added N_2 and NH_3 at constant T_{fil}

Relative number densities of H atoms (henceforth represented by [H]) and CH_3 radicals ($[CH_3]$) were measured by $2+1$ REMPI, as a function both of added $NH_3(N_2)$ and T_{fil}. Figures 3 and 4 show experimentally measured [H] and

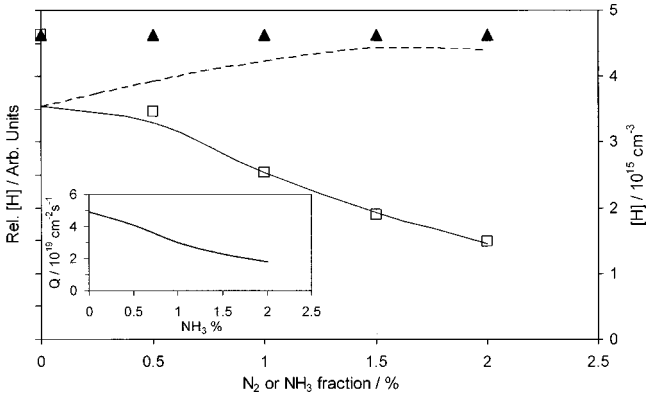

FIG. 3. Experimentally measured H atom relative number densities as a function of added N_2 (▲) and NH_3 (□), for 1% CH_4 in H_2 mixtures (flow rate=100 sccm, total pressure=20 Torr) and $T_{fil}=2573$ K, measured at $d=4$ mm beneath the midpoint of the lower edge of the coiled filament. The dashed curve shows the calculated variation in absolute [H] (right-hand side scale), assuming fixed values of $Q=4.92\times 10^{19}\ cm^{-2}\ s^{-1}$, $T_{nf}=2075$ K, together with the previously established (see Ref. 27) d dependence of T_{gas}. The solid curve shows a fit to the NH_3 data obtained by assuming that Q declines with added NH_3 as shown in the inset. Experimental and theory [assuming $Q(NH_3)$ as in the inset] are scaled so as to match for 1% added NH_3.

$[CH_3]$ values, as a function of added N_2 and NH_3, for a 1% CH_4 in H_2 mixture (flow rate=100 sccm, total pressure =20 Torr) and $T_{fil}=2573$ K, measured at a distance $d=4$ mm beneath the midpoint of the lower edge of the coiled filament. Clearly, given the discussion in the preceding section, it was necessary to increase the power supplied to the HF progressively as the NH_3 input mole fraction increased in order to maintain a constant T_{fil}.

Interpreting these, and subsequent, experimental data builds on our previous modeling of the gas-phase chemistry occurring in activated CH_4/H_2 and C_2H_2/H_2 gas mixtures in this same HF-CVD reactor.[29,32,33] The reactor (with no substrate present) is represented in Cartesian coordinates with the z axis parallel to the direction of feedstock gas flow

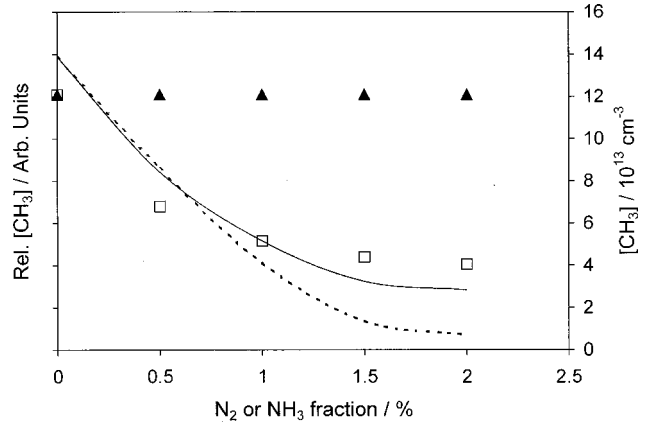

FIG. 4. Experimentally measured CH_3 radical relative number densities as a function of added N_2 (▲) and NH_3 (□), for 1% CH_4 in H_2 mixture with total flow rates, pressure and T_{fil} as in Fig. 3, again measured at $d=4$ mm. The dashed and solid curves show the calculated variation in absolute $[CH_3]$ (right-hand side scale) assuming, respectively, the same fixed and $[NH_3]$ dependent values for Q as in Fig. 3 with, again, the experimental and model outputs set to match for 1% added NH_3.

(input→output) and perpendicular to the filament. The center axis of the filament defines the y axis, and x is orthogonal to both the filament axis and the direction of gas flow. The modelling considers the volume bounded by $x=\pm 16$ mm, $y=\pm 18$ mm, and $z=\pm 26$ mm, with the point (0, 0, 0) defining the center of the filament. $d=0$ corresponds to the point (0, 0, 1.5 mm), since the coiled filament has diameter 3 mm. The points (0, 0, −26 mm) and (0, 0, +26 mm) define the gas inlet and outlet positions, where the gas temperature is set to $T_{\text{gas}}=450$ K. The present calculations include two refinements as compared with those reported previously.[32,33] First, the T_{gas} values at all other boundaries of the numerical grid (hitherto constrained to be 450 K also) were now chosen more carefully so as to ensure that the temperature distribution far from the HF exhibits near spherical symmetry. Second, $\Delta T=T_{\text{fil}}-T_{\text{nf}}$, the temperature drop between the HF surface and the immediate gas phase, was allowed to be a function of T_{fil}, varying from $\Delta T=500$ K when $T_{\text{fil}}=2700$ K, through 475 K for $T_{\text{fil}}=2500$ K and down to 350 K at $T_{\text{fil}}=2200$ K.[39] Initial 3D simulations assume experimental values for T_{fil}, gas pressure and flow rate, a net H atom production rate at the filament ($Q=4.92\times10^{19}$ cm^{-2} s^{-1}), a near filament gas temperature ($T_{\text{nf}}=2075$ K), and a d dependence for T_{gas} consistent with our previous characterisations of H_2, CH_4/H_2, and C_2H_2/H_2 gas-phase chemistry in this reactor.[27,29,32,33]

In the case of N_2 additions, such modeling accords with experiment in finding that both [H] and [CH_3] are insensitive to added N_2. This result can be readily understood by inspecting the calculated temperature (and thus position) dependent interconversion rates and number densities for the various participating species for the case of a 1% CH_4/1% N_2/H_2 gas mixture. These show N_2 to be an essentially inert spectator, with a predicted fractional dissociation [N]/[N_2] $<10^{-7}$ even at $T_{\text{gas}}\sim2000$ K, i.e., very close to the HF. This reflects the extreme bond strength of N_2; [D_0(N≡N) $=941.6$ kJ mol^{-1}].[40] Further simulations, in which this ratio was arbitrarily increased (such as could apply in the event that N_2 dissociation was catalyzed on the HF surface or, in the case of microwave activation, as a result of nonthermal plasma chemistry) indicate that the [N]/[N_2] ratio would have to be at least 100 times higher to cause a discernible reduction in the measured [CH_3].

In contrast, Figs. 3 and 4 clearly show that both [H] and [CH_3] are sensitive to NH_3 additions. The calculated z dependent interconversion rates and number densities for major species present in an HF activated 1% CH_4/1% NH_3/H_2 gas mixture (Figs. 5 and 6, respectively) show this nitrogen containing precursor to be intimately involved in the high-temperature gas-phase chemistry—a reflection, at least in part, of the much weaker N—H bond strength [D_0(H_2N—H) $=443.9$ kJ mol^{-1}].[41] Temperature and pressure dependent rate constants, $k(T,P)$, for the 100 elementary steps (50 forward and back reactions) underpinning the H/C/N gas phase chemistry are taken from the GRI-Mech 3.0 reaction mechanism.[31] These were supplemented by one additional reversible step

$$H+H_2CN\rightleftharpoons H_2+HCN. \tag{7}$$

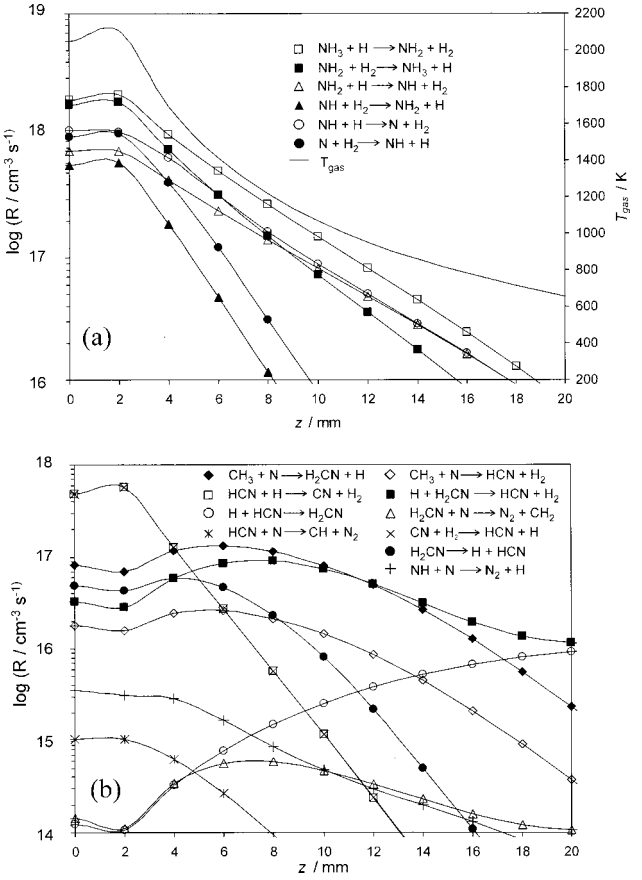

FIG. 5. Semilogarithmic plots showing calculated rates, R (in molecules cm^{-3} s^{-1}, left-hand side scale), for (a) the H-shift reactions $NH_x+H\rightleftharpoons NH_{x-1}+H_2$ (10) and (b) selected other reactions involving N containing species, for an HF activated 1% CH_4/1% NH_3/H_2 mixture ($T_{\text{fil}}=2573$ K) plotted as a function of z (with $x=y=0$). The calculations assume $Q=2\times10^{19}$ cm^{-2} s^{-1}, $T_{\text{nf}}=2100$ K and the shown z dependence of T_{gas} [(a), right-hand side scale].

All species and reactions involving O atoms were excluded. Kinetic data for the strongly exothermic reaction (7) appears to be restricted to one preliminary study which suggested a rate constant $k_7>7\times10^{-11}$ cm^3 s^{-1} at 298 K, i.e., some 50% faster than that for the better documented reaction of N atoms with H_2CN.[42] Since, as Fig. 6(a) shows, the H:N atom concentration ratio in the present environment is $\sim10^2$ at all z it is clearly necessary to include a realistic parameterization of reaction (7) in the present modeling. Lacking other knowledge, we thus presume it to proceed at or near the gas kinetic collision rate with $k(T,P)$ the same as for the (documented)[31] analogue

$$H+HCO\rightleftharpoons H_2+CO. \tag{8}$$

Inclusion of reaction (7) has rather little effect on the near filament HCN and H_2CN concentrations but, in the cooler regions, reduces the steady state concentration of H_2CN by some four orders of magnitude causing a ~25% increase in the calculated HCN concentration.

The dashed lines in Figs. 3 and 4 show absolute H atom and CH_3 radical number densities predicted by these initial 3D simulations. Though the model succeeds in capturing the experimentally measured trend in [CH_3] quite well, it con-

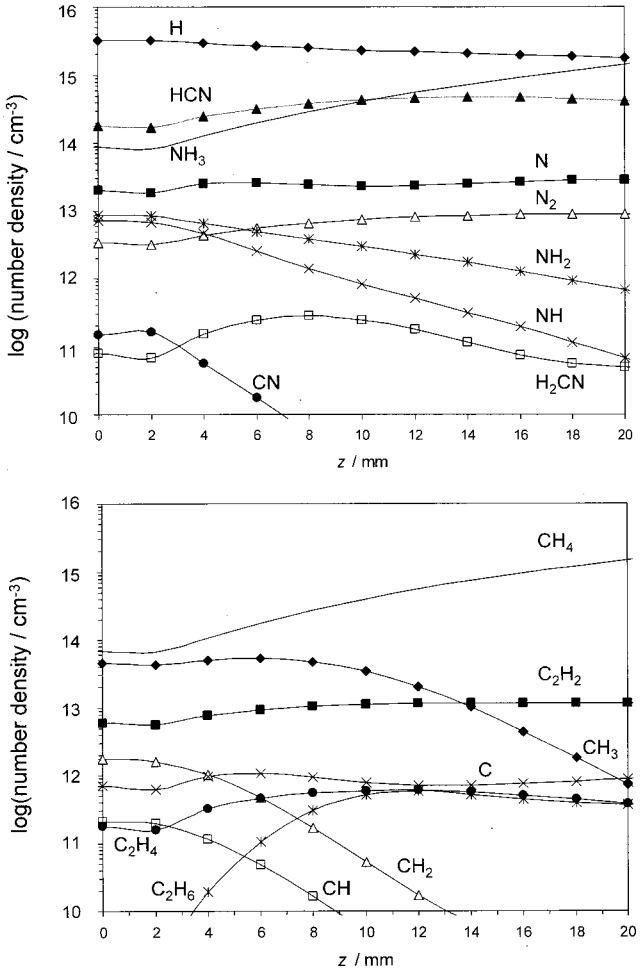

FIG. 6. Calculated number densities of (a) H, N, N_2, NH_b ($b=1-3$), and other of the more abundant N containing species and (b) C atoms and the more abundant C_1 and C_2 hydrocarbon species in an HF activated 1% CH_4/1% NH_3/H_2 mixture, plotted as a function of z (with $x=y=0$), assuming the same Q, T_{nf} and $T_{gas}(z)$ values as in Fig. 5.

spicuously fails to reproduce the observed variation of [H] with added NH_3. Given the magnitudes and temperature dependences of the rates of reactions that produce and consume H atoms (Fig. 5), the predicted modest increase in [H] upon addition of trace amounts of NH_3 is perhaps surprising. Numerous previous studies[33,43] have shown that hydrocarbon based ''H-shifting'' reactions of the form

$$CH_x + H \rightleftharpoons CH_{x-1} + H_2 \tag{9}$$

are the dominant H atom loss mechanism in the hotter regions of HF activated CH_4/H_2 gas mixtures. Careful inspection of the various T_{gas} (and thus z) dependent reaction rates and species number densities shown in Figs. 5 and 6 shows that addition of NH_3 introduces a corresponding set of H-shifting reactions of the form:

$$NH_x + H \rightleftharpoons NH_{x-1} + H_2 \tag{10}$$

that compete with, and suppress, the reaction sequence (9). For the specific case of a 1% CH_4/1% NH_3/H_2 gas mixture, the two sets of H-shift reactions (9) and (10) make comparable contributions to the overall H atom loss rate in the near filament region. However, both consumption rates are an order of magnitude slower than the presumed H atom production rate, Q—hence the comparative insensitivity of [H] predicted upon addition of NH_3.

To accommodate the experimentally observed reduction of [H] upon adding NH_3, it is necessary to assume that N termination of the HF surface causes not only an increase in emissivity but also a reduction in Q. The inset to Fig. 3 shows the functional form of $Q(NH_3)$, at the prevailing filament temperature ($T_{fil}\sim 2573$ K), that we assume in order that the calculated H atom number densities show a reasonable match to the experimentally measured variation in [H] with added NH_3. Such a decrease in Q with increasing NH_3 is plausible, given the previous conclusions that NH_3 addition leads to modification (''N termination'') of the HF surface and of its emissivity. The final comparison between the measured relative H atom and CH_3 radical number densities (□ in Figs. 3 and 4) and the corresponding absolute number densities returned by the model (shown by the solid lines) have been scaled so as to match at 1% added NH_3.

Before proceeding further, it is worth commenting on the values of Q used in this, and previous,[29,30,32,33] modeling of the gas-phase chemistry occurring in the Bristol HF-CVD reactor, which are about one tenth of those estimated in a previous investigation of the way the temperature of a Ta HF varied as a function of CH_4/H_2 input gas mixing ratio and the power supplied to the filament. Li *et al.*[37] derived values for Q, as a function of T_{fil}, by estimating the power consumed in H_2 dissociation on both clean and ''poisoned'' Ta filaments (i.e., HFs envisaged as having a pure TaC surface, and a graphitic overcoat, respectively). Energy balance considerations, together with the assumption that the clean and poisoned surfaces exhibit their respective limiting emissivities, allowed estimation of $Q(T_{fil})$ values.[37] However, if the surface of a carburized filament is actually partially overcoated TaC (as deduced in the present study)—albeit with a coverage that varies with T_{fil} and with the CH_4/H_2 mixing fraction, then the mean emissivities of the clean and poisoned surfaces would be more similar than hitherto assumed and the Q values so derived would necessarily have to be reduced.

C. Gas phase H atom and CH_3 radical number densities in a 1% CH_4/1% NH_3/H_2 gas mixture as a function of T_{fil}

Figures 7 and 8 show, respectively, the H atom and CH_3 radical relative number densities measured 4 mm from the HF as a function of T_{fil} for a 1% CH_4/H_2 input gas mixture, with and without 1% added NH_3. As in previous studies of pure H_2 and CH_4/H_2 gas mixtures,[27] the H atom number density near the HF (Fig. 7) is seen to increase near exponentially across the T_{fil} range of interest, i.e., $[H]\sim\exp(-\Delta H_{diss}/RT_{fil})$, where $\Delta H_{diss}\sim 240$ kJ mol^{-1} is the enthalpy for H atom formation on the HF surface and R is the gas constant. Figure 7 also confirms that the previously observed reduction in [H] upon addition of NH_3 (Fig. 3) extends to all T_{fil}. To stiffen the modeling, we assume that the previously deduced functional form of Q upon NH_3 addition [at $T_{fil}=2573$ K, shown in the inset to Fig. 3, and henceforth written as $Q_0(NH_3)$] applies at all T_{fil} values relevant to the

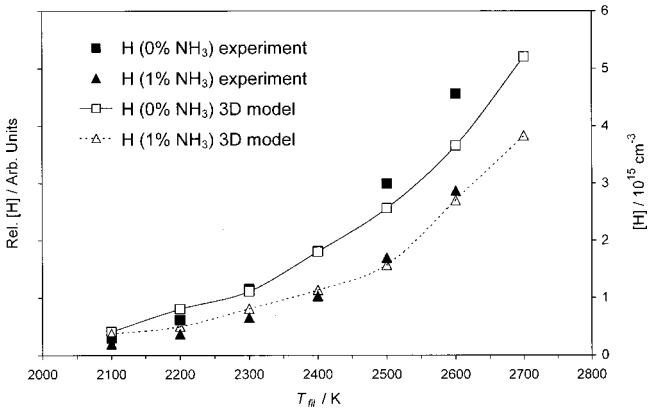

FIG. 7. H atom relative number densities measured at a distance $d=4$ mm from the HF as a function of $T_{\rm fil}$ for a 1% CH_4/H_2 input gas mixture (flow rate=100 sccm, total pressure=20 Torr), with and without 1% added NH_3 (▲ and ■, respectively). The open squares joined by the solid curve (——□——) show the result of the 3D model calculations for the ammonia-free gas-phase chemistry using Eq. (11) and $Q_0=3.6\times10^{24}$ cm^{-2} s^{-1}. The corresponding model output for the case of 1% added NH_3, assuming $Q(1\%\ NH_3)/Q(0\%\ NH_3)=0.57$, is shown by the open triangles and dashed line (— — —△— — —). For both data sets, experiment and theory are scaled as in Fig. 3 (but at $T_{\rm fil}=2600$ K).

present work. We also assume that the exponential relationship between Q and $T_{\rm fil}$ identified in the earlier studies of pure H_2 dissociation in this same HF reactor is applicable at all NH_3 partial pressures used here. Thus, we arrive at the following relationship for Q at any relevant $T_{\rm fil}$ and added NH_3 fraction:

$$Q(T_{\rm fil},NH_3)=Q_0(NH_3)\cdot\exp(-\Delta H_{\rm diss}/RT_{\rm fil}), \qquad (11)$$

involving just one adjustable parameter $Q_0(NH_3=0\%)$—henceforth written simply as Q_0—with which to match all of the REMPI measurements of [H] and $[CH_3]$ at different $T_{\rm fil}$ and gas mixing ratios.

Figure 8 displays the resulting comparison between CH_3 radical relative number densities measured at a distance $d=4$ mm from the HF, as a function of $T_{\rm fil}$, using a 1% CH_4/H_2 input gas mixture with and without addition of 1% NH_3, and those calculated using Eq. (11), a ratio $Q(1\%\ NH_3)/Q(0\%\ NH_3)=0.57$ (as in the inset to Fig. 3), and $Q_0=3.6\times10^{24}$ cm^{-2} s^{-1}. A range of Q_0 values were investigated, and this value chosen so as to reproduce the local maximum in $[CH_3]$ for the 1% CH_4/1% NH_3/H_2 gas mixture at $T_{\rm fil}\sim2500$ K, and the marked decrease in $[CH_3]$ at higher $T_{\rm fil}$ values. This value also reproduces the smooth rise in $[CH_3]$ with increasing $T_{\rm fil}$ found experimentally when using a standard 1% CH_4/H_2 gas mixture[29] and the observed saturation of $[CH_3]$ reported when using such mixtures at very high $T_{\rm fil}$.[44]

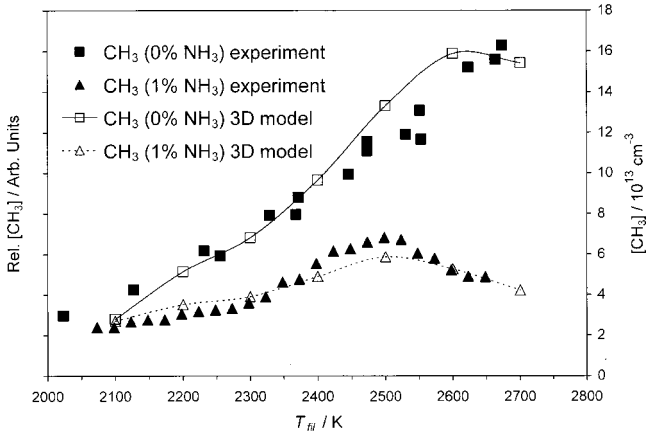

FIG. 8. CH_3 radical relative number densities measured under the same experimental conditions as in Fig. 7, with and without 1% added NH_3 (▲ and ■, respectively). As in Fig. 7, the 3D model outputs using Eq. (11) and $Q_0=3.6\times10^{24}$ cm^{-2} s^{-1}, with and without NH_3 additions, are depicted by the dashed (— — —△— — —) and solid (——□——) curves, respectively. Experiment and theory are scaled to one another using the same normalization for 1% added NH_3 as employed in Fig. 4, but at $T_{\rm fil}=2600$ K.

The calculated temperature (and thus position) dependent species number densities (Fig. 6) and inter-conversion rates (Fig. 5) enable construction of a reasonably self-consistent picture of the gas-phase transformations occurring in a HF-CVD reactor operating at typical modest filament temperatures when NH_3 is added to a hydrocarbon/H_2 gas mixture. Input CH_4 molecules pass through a multistep sequence of reactions en route to stable products C_2H_2 and HCN, thereby depleting the number densities of CH_x species both near the HF and in the surrounding volume extending out to distances where any substrate would normally be positioned in a diamond growth experiment. HCN acts as a sink for input NH_3 molecules also. The present studies show that NH_3 additions to an activated CH_4/H_2 gas mixture cause reductions in the CH_x number density close to the HF in two ways. First, the addition of NH_3 introduces additional purely gas phase CH_x loss processes, most importantly irreversible transformation of CH_3 radicals to HCN through reaction with N atoms in the vicinity of the HF. Secondly, and even more importantly, NH_3 additions are shown to cause modifications of the HF surface, increasing its emissivity and thus lowering $T_{\rm fil}$ (for a given input power) and reducing its efficiency for catalyzing H_2 dissociation, even if $T_{\rm fil}$ is maintained constant. Given the critical role of methyl radicals in diamond growth in such HF-CVD reactors,[43] the deduced reduction in $[CH_3]$ is wholly consistent with previous reports[21] of reduced diamond deposition rates when the input fraction of NH_3 begins to approach that of CH_4.

D. NH radical number densities and spatial profiles in 1% $CH_4/x\%$ NH_3/H_2 gas mixtures

The modeling of the gas-phase chemistry summarized in the form of z dependent species concentrations and elementary reaction rates in Figs. 5 and 6 suggests that the number density of NH radicals in the vicinity of the HF should be sufficient ($>10^{12}$ cm^{-3}) to permit their detection by a sensitive absorption method like CRDS.[25,26] Unlike REMPI, such measurements offer a route to *absolute* column densities, and thus provide a further test of the absolute values of Q, and their dependence on $T_{\rm fil}$ and $[NH_3]$, returned by the gas-phase chemistry modeling. Figure 9, which displays a correct cavity ring down (CRD) spectrum of part of the Q branch region of the NH(A-X) origin band at ~336 nm recorded along a column parallel to, and at $d=1$ mm below, the HF while using a 1% CH_4/10% NH_3/H_2 gas mixture, verifies

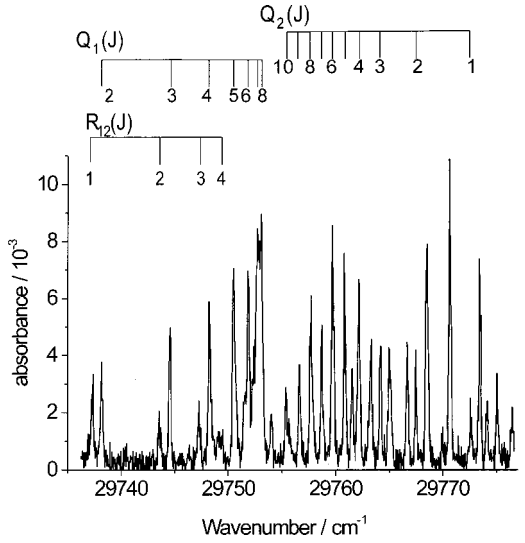

FIG. 9. CRD spectrum of NH radicals in the viewing column parallel to, and at a distance $d=1$ mm below, the bottom of a HF maintained at $T_{\mathrm{fil}}=2473$ K for a 1% CH_4/10% NH_3/H_2 input mixture (flow rate $=100$ sccm, total pressure$=20$ Torr), monitored via the (0,0) band of the $A\,^3\Pi-X\,^3\Sigma^-$ transition.

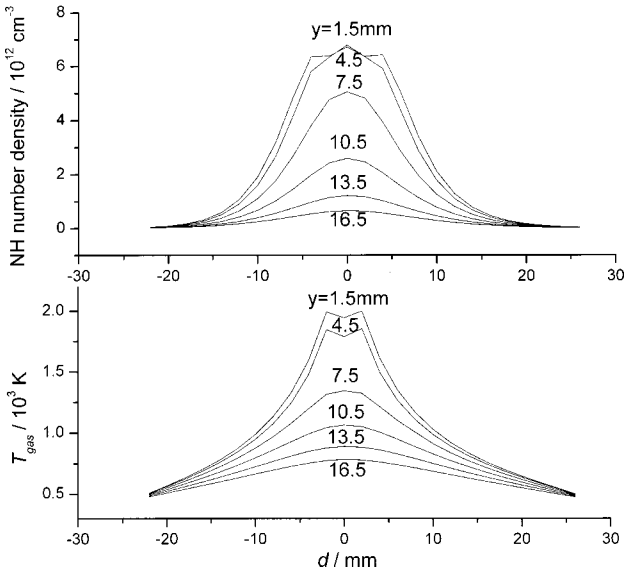

FIG. 10. Plots showing the variation in (a) the calculated z dependence of the absolute NH number densities for a HF activated 1% CH_4/10% NH_3/H_2 gas mixture ($T_{\mathrm{fil}}=2473$ K) and (b) T_{gas}, as a function of y, assuming $Q(6\times10^{18}\ \mathrm{cm^{-2}\,s^{-1}})$ and T_{nf} (1900 K). $y=0$ represents the midpoint of the long axis of the HF.

such expectations though to obtain a signal to noise ratio of the quality shown in Fig. 9 it was helpful to employ this high NH_3 mixing fraction. We find no evidence of any comparable absorption when using a 1% CH_4/10% N_2/H_2 gas mixture, consistent with previous conclusions regarding the unreactivity of N_2 under such mild conditions of HF activation. Line assignments were made using literature values of the spectroscopic constants for the $v=0$ levels of the $A\,^3\Pi$ and $X\,^3\Sigma^-$ states of NH.[45] Simulations of the entire origin band show much reduced line density at higher frequency, and subsequent NH column density determinations all involved monitoring absorption associated with the rotational lines $R_1(2)$ and $R_1(3)$ at, respectively, 29 809.8 $\mathrm{cm^{-1}}$ and 29 846.3 $\mathrm{cm^{-1}}$. These lines were selected on the basis of their intrinsic linestrengths, their isolation from other spectral features, and the fact that they probe levels with significant population at the prevailing gas temperatures. As with the REMPI measurements, number densities were determined as a function of input NH_3 mole fraction and as a function of radial distance d from the lower edge of the coiled filament.

The change in the ring down rate coefficient, Δk, was measured on a point by point basis across the linewidth of the chosen probe transition, thereby yielding an integrated absorbance per pass, $\alpha\ell$ [recall Eq. (1)], associated with that transition under the prevailing experimental conditions. CRDS is a line-of-sight technique, so this measured absorbance is a convolution over the position dependent NH number density and gas temperature along the column. In order to compare the measured value with the model predictions, it is necessary to perform an analogous convolution of the model output. This procedure treats the space surrounding the filament in cells of cross section 1 mm$\times$1 mm and length $\Delta y=3$ mm. The first step involves determination of the mean value of [NH] and T_{gas} in each of these cells from the model output. Figures 10(a) and 10(b) show an illustrative set of such data, in the form of calculated absolute NH number densities and T_{gas} values, as a function of vertical distance z, for a number of different y (where $y=0$ corresponds to the midpoint of the long axis of the HF). These model calculations employ Q and T_{nf} values ($6\times10^{18}\ \mathrm{cm^{-2}\,s^{-1}}$, and 1990 K, respectively) that are sensible extrapolations of the corresponding values used above when modeling the effects of smaller NH_3 additions. Stage two involves simulation of the complete NH(A-X) origin band for each relevant T_{gas} value using the program PGOPHER,[46] from which we can calculate the fraction, p, of the total band oscillator strength, f_{00}—given as $(77.1\pm2.6)\times10^{-4}$ in Ref. 47—that is associated with the monitored transition at that particular value of T_{gas}. Calculating p in this way ensures proper allowance of both the linestrength and Boltzmann factors. The deduced fraction of f_{00} and the integrated absorption coefficient of the line of interest are related by[48]

$$\int_{\mathrm{line}}\alpha_v\,dv=\frac{e^2}{4\varepsilon_0 mc}[\mathrm{NH}]_{v=0}f_{00}p, \tag{12}$$

where e and m are, respectively, the charge and mass of the electron, and ε_0 is the vacuum permittivity. The number density of NH radicals in the probed ground vibrational level, $[\mathrm{NH}]_{v=0}$, is obtained from the calculated total NH concentration using the vibrational partition function at the appropriate T_{gas}. The absorbance predicted by the gas phase simulations is then obtained by summing the calculated T_{gas} dependent contributions (12) from each cell along the entire viewing column. Figure 11 displays the measured and predicted d dependence of the NH absorbance for the case of a 1% CH_4/5% NH_3/H_2 gas mixture with $T_{\mathrm{fil}}=2473$ K, monitored via the $R_1(2)$ and $R_1(3)$ transitions; the insets show the calculated temperature dependence of p, the fraction of the total band oscillator strength carried by these respective

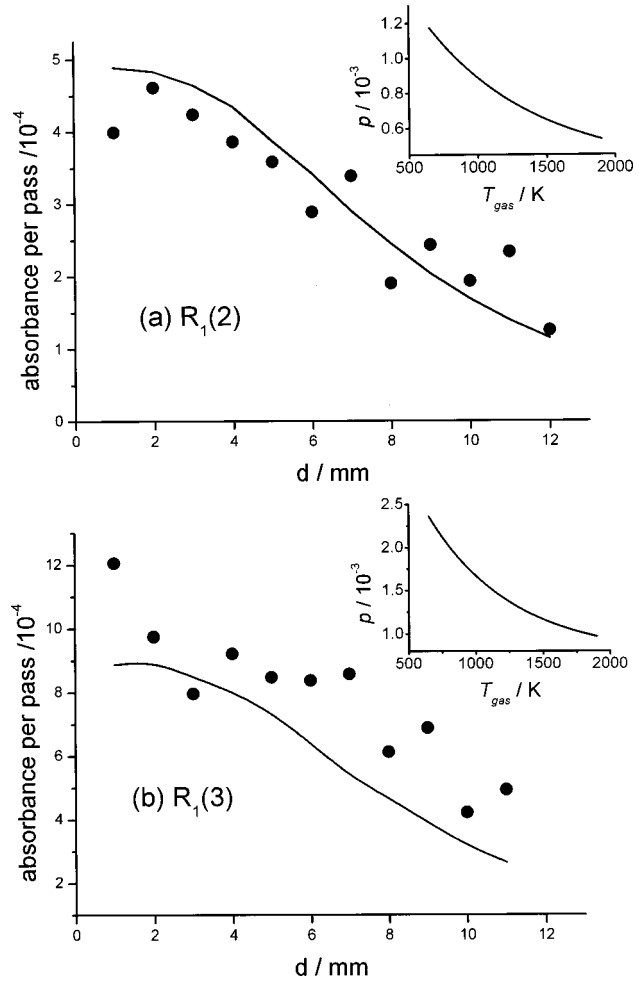

FIG. 11. Measured (●) and predicted (——) d dependence of the NH absorbance per pass for a 1% CH_4/5% NH_3/H_2 gas mixture (flow rate $=100$ sccm, total pressure$=20$ Torr) with $T_{fil}=2473$ K. The former data were obtained by monitoring (a) the $R_1(2)$ and (b) the $R_1(3)$ transitions of the NH$(A-X)$ origin band, respectively; the insets show the calculated temperature dependence of p, the fraction of the total band oscillator strength carried by these respective transitions.

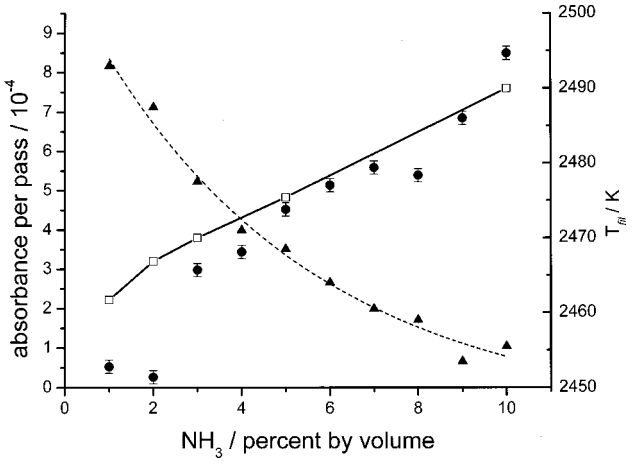

FIG. 12. NH absorbance per pass (●) measured at $d=2$ mm in an HF activated 1% $CH_4/x\%$ NH_3/H_2 gas mixture as a function of input NH_3 fraction ($x=0\%-10\%$), monitored via the $R_1(2)$ transition at 29 809.8 cm^{-1}. The input power to the HF was held constant at 85 W, with the result that the measured T_{fil} declined with increasing NH_3 as shown (▲, and right-hand side axis). The dashed curve through the temperature data is simply to guide the eye. The open symbols linked by the solid line (——□——) show calculated NH absorbances using Eq. (12) together with [NH] values returned by the 3D model assuming the following values of T_{nf} and Q: $x=1\%$, $T_{nf}=2020$ K, $Q=1.8\times10^{19}$ cm^{-2} s^{-1}; $x=2\%$, $T_{nf}=2010$ K, $Q=1.1\times10^{19}$ cm^{-2} s^{-1}; $x=3\%$, $T_{nf}=2000$ K, $Q=7.7\times10^{18}$ cm^{-2} s^{-1}; $x=5\%$, $T_{nf}=1990$ K, $Q=6\times10^{18}$ cm^{-2} s^{-1}; $x=10\%$, $T_{nf}=1980$ K, and $Q=4.8\times10^{18}$ cm^{-2} s^{-1}.

transitions. Clearly, the level of agreement in both cases (to within a factor of two in the implied absolute number densities, at all d) provides strong support for the validity of the foregoing modeling of the gas-phase chemistry of H/C/N containing mixtures in a HF-CVD reactor, and the spatially resolved absolute number densities returned by the simulations for all major species. Figure 12 shows absorbance due to NH radicals, monitored via the $R_1(2)$ transition, measured at $d=2$ mm in HF activated 1% $CH_4/x\%$ NH_3/H_2 gas mixtures ($x=0\%-10\%$) with a constant input power to the HF; T_{fil} thus declines slightly with increasing x as shown. Unsurprisingly, the measured NH absorbance scales with input NH_3 mole fraction. Once again, the essentially quantitative agreement with the corresponding absorbance values predicted through use of Eq. (12), together with NH number density values returned by the 3D model assuming the plausible near filament temperatures, T_{nf}, and $Q(NH_3)$ values consistent with extrapolation of the trend shown in the inset to Fig. 3 (detailed in the caption to Fig. 12), suggests that our analysis correctly captures the main elements of the gas-phase chemistry prevailing in HF activated $CH_4/NH_3/H_2$ gas mixtures.

IV. CONCLUSIONS

REMPI spectroscopy has been used to provide spatially resolved relative H atom and CH_3 radical number densities in a HF-CVD reactor operating with a 1% $CH_4/x/H_2$ gas mixture, where x represents known controlled additions of N_2 or NH_3. These relative number density measurements have been placed on an absolute scale via 3D modeling of the chemistry prevailing in such HF activated gas mixtures. Experiment and theory both show that N_2 is unreactive under the prevailing experimental conditions, while NH_3 additions have a major effect on the gas-phase chemistry and composition. Specifically, the introduction of NH_3 introduces an additional sequence of H-shift reactions (10) that result in the formation of N atoms with steady state concentrations $\sim5\times10^{13}$ cm^{-3} in the hotter regions of the reactor. These participate in reactions that cause irreversible conversion of CH_3 radicals to HCN—thereby reducing the number density of free hydrocarbon species available to participate in diamond growth. This reduction in $[CH_3]$ as a result of competing gas-phase chemistry is shown to be compounded by NH_3 induced modifications to the HF and, particularly, its ability to promote surface catalyzed H_2 dissociation (parametrized by a net H atom production rate, Q). The deduced reductions in $[CH_3]$ are entirely consistent with previous reports (Ref. 16) that the rate of diamond deposition from $CH_4/NH_3/H_2$ gas mixtures is much reduced when the input fraction of NH_3 becomes comparable to that of CH_4.

Further support for the validity of the modeling of the gas-filament surface and pure gas-phase chemistry is provided by our finding of very good agreement between the calculated spatial distribution of NH radical number densities in a HF activated 1% CH_4/5% NH_3/H_2 gas mixtures and the absolute NH column densities in such mixtures obtained by monitoring selected rovibronic transitions within the NH(A-X) origin band by CRDS. Finally, we note that the modeling predicts CN radical concentrations $<10^9$ cm^{-3} at all realistic filament—substrate distances. If, as has been speculated, N incorporation into a growing diamond film involves CN (instead of CH_3) addition to a vacant surface site, the deduced paucity of gas-phase CN radicals in such HF activated mixtures could provide a ready explanation for the reported low N doping efficiencies.[2,3,18,49] Clearly, if such is the case, the present analyses suggest that N incorporation would be enhanced by use of higher N/H ratios in the input gas mixture (thereby increasing the CN:CH_3 ratio). Such is generally consistent with observations, whereby improved N doping efficiencies have been found when using higher activation efficiencies (e.g., microwave plasma enhanced CVD) and $CH_4/N_2/H_2$ and $CH_4/CO_2/N_2$ gas mixtures.[14]

ACKNOWLEDGMENTS

The Bristol group are grateful to the EPSRC for equipment grants and for the award of a Senior Research fellowship (M.N.R.A.) and studentships (J.A.S. and J.B.W.). The authors are also grateful to the Royal Society for a Joint Project Grant to enable the Bristol–Moscow collaboration and to Dr. P. W. May, Dr. S. A. Redman, Dr. C. M. Western, and K. N. Rosser for their many and varied contributions to this work.

[1] J. Mort, M. A. Machonkin, and K. Okumura, Appl. Phys. Lett. **59**, 3148 (1991).
[2] A. Badzian, T. Badzian, and S.-T. Lee, Appl. Phys. Lett. **62**, 3432 (1993).
[3] S. Jin and T. D. Moustakas, Appl. Phys. Lett. **63**, 2354 (1993); **65**, 403 (1994).
[4] R. Locher, C. Wild, N. Herres, D. Behr, and P. Koidl, Appl. Phys. Lett. **65**, 34 (1994).
[5] R. Samlenski, C. Hauge, R. Brenn, C. Wild, R. Locher, and P. Koidl, Appl. Phys. Lett. **67**, 2798 (1995).
[6] W. Muller-Sebert, E. Worner, F. Fuchs, C. Wild, and P. Koidl, Appl. Phys. Lett. **68**, 759 (1996).
[7] C. Wild, R. Locher, and P. Koidl, Mater. Res. Soc. Symp. Proc. **416**, 75 (1996).
[8] G. Z. Cao, J. J. Schermer, W. L. P. van Enckevort, W. A. L. M. Elst, and L. J. Giling, J. Appl. Phys. **79**, 1357 (1996).
[9] T. Vandevelde, H. Nesladek, C. Quaeyhagens, and L. M. Stals, Thin Solid Films **308**, 154 (1997).
[10] J. Michler, J. Stiegler, Y. von Kaenel, P. Moeckli, W. Dorsch, D. Stenkamp, and E. Blank, J. Cryst. Growth **170**, 404 (1997).
[11] A. Afzal, C. A. Rego, W. Ahmed, and R. I. Cherry, Diamond Relat. Mater. **7**, 1033 (1998).
[12] Z. Yu, U. Karlsson, and A. Flodstrom, Thin Solid Films **342**, 74 (1999).
[13] J. Stiegler, A. Bergmaier, J. Michler, S. Laufer, G. Dollinger, and E. Blank, Thin Solid Films **352**, 29 (1999).
[14] V. Baranauskas, S. F. Durrant, M. C. Tosin, A. C. Peterlevitz, B. B. Li, and S. G. Castro, Thin Solid Films **355-6**, 157 (1999).
[15] M. Park, A. T. Sowers, C. L. Rinne, R. Schlesser, L. Bergman, R. J. Nemanich, Z. Sitar, J. J. Hren, J. J. Cuomo, V. V. Zhirnov, and W. B. Choi, J. Vac. Sci. Technol. B **17**, 734 (1999).
[16] A. T. Sowers, B. L. Ward, S. L. English, and R. J. Nemanich, J. Appl. Phys. **86**, 5162 (1999).
[17] O. Elmazria, J. Bougdira, H. Chatei, L. De Pouques, M. Remy, and P. Alnot, Thin Solid Films **374**, 27 (2000).
[18] K. Iakoubovskii, G. J. Adriaenssens, and Y. K. Vohra, Diamond Relat. Mater. **10**, 485 (2001) and references therein.
[19] V. I. Polyakov, A. I. Rukovishnikov, N. M. Rossukanyi, and V. G. Ralchenko, Diamond Relat. Mater. **10**, 593 (2001).
[20] V. M. Ayres, M. Farhan, D. Spach, J. Bobbitt, J. A. Majeed, B. F. Wright, B. L. Wright, J. Asmussen, M. G. Kanatzidis, and T. R. Bieler, J. Appl. Phys. **89**, 6062 (2001).
[21] P. W. May, P. R. Burridge, C. A. Rego, R. S. Tsang, M. N. R. Ashfold, K. N. Rosser, R. E. Tanner, D. Cherns, and R. Vincent, Diamond Relat. Mater. **5**, 354 (1996).
[22] R. S. Tsang, C. A. Rego, P. W. May, M. N. R. Ashfold, and K. N. Rosser, Diamond Relat. Mater. **6**, 247 (1997).
[23] S. M. Leeds, P. W. May, M. N. R. Ashfold, and K. N. Rosser, Diamond Relat. Mater. **8**, 226 (1999).
[24] A. O'Keefe and D. A. G. Deacon, Rev. Sci. Instrum. **59**, 2544 (1988).
[25] M. D. Wheeler, S. M. Newman, A. J. Orr-Ewing, and M. N. R. Ashfold, J. Chem. Soc., Faraday Trans. **94**, 337 (1998).
[26] G. Berden, R. Peeters, and G. Meijer, Int. Rev. Phys. Chem. **19**, 565 (2000).
[27] S. A. Redman, C. Chung, K. N. Rosser, and M. N. R. Ashfold, Phys. Chem. Chem. Phys. **1**, 1415 (1999).
[28] J. A. Smith, M. A. Cook, S. R. Langford, S. A. Redman, and M. N. R. Ashfold, Thin Solid Films **368**, 169 (2000).
[29] J. A. Smith, E. Cameron, M. N. R. Ashfold, Y. A. Mankelevich, and N. V. Suetin, Diamond Relat. Mater. **10**, 358 (2001).
[30] Y. A. Mankelevich, A. T. Rakhimov, and N. V. Suetin, Diamond Relat. Mater. **7**, 1133 (1998).
[31] G. P. Smith, D. M. Golden, M. Frenklach, N. W. Moriarty, B. Eiteneer, M. Goldenberg, C. T. Bowman, R. K. Hanson, S. Song, W. C. Gardiner, Jr., V. V. Lissianski, and Z. Qin, http://www.me.berkeley.edu/gri_mech/
[32] Y. A. Mankelevich, N. V. Suetin, M. N. R. Ashfold, J. A. Smith, and E. Cameron, Diamond Relat. Mater. **10**, 364 (2001).
[33] M. N. R. Ashfold, P. W. May, J. R. Petherbridge, K. N. Rosser, J. A. Smith, Y. A. Mankelevich, and N. V. Suetin, Phys. Chem. Chem. Phys. **3**, 3471 (2001).
[34] Y. S. Touloukian and D. P. de Witt, in *Thermal Radiative Properties: Nonmetallic Solids, Thermophysical Properties of Matter*, edited by Y. S. Touloukian and C. Y. Ho (Plenum, New York, 1972), Vol. 8, p. 811.
[35] M. Sommer and F. W. Smith, J. Vac. Sci. Technol. A **9**, 1134 (1991).
[36] D. Morel and W. Hänni, Diamond Relat. Mater. **7**, 826 (1998).
[37] D. M. Li, R. Hernberg, and T. Mäntylä, Diamond Relat. Mater. **7**, 1709 (1998).
[38] H. F. Winters, H. Seki, R. R. Rye, and M. E. Coltrin, J. Appl. Phys. **76**, 1228 (1994).
[39] Y. A. Mankelevich, N. V. Suetin, J. A. Smith, and M. N. R. Ashfold, Diamond Relat. Mater **11**, 567 (2002).
[40] M. W. Chase, Jr., *NIST-JANAF Thermochemical Tables*, 4th ed., (1998), Monograph No. 9, 1-1951 (American Institute of Physics, New York, 1998).
[41] D. H. Mordaunt, M. N. R. Ashfold, and R. N. Dixon, J. Chem. Phys. **104**, 6460 (1996).
[42] F. L. Nesbitt, G. Marston, and L. J. Stief, J. Phys. Chem. **94**, 4946 (1990).
[43] D. G. Goodwin and J. E. Butler, in *Handbook of Industrial Diamonds and Diamond Films*, edited by M. A. Prelas, G. Popovici, and L. K. Bigelow (Marcel Dekker, New York, 1998), pp. 527–581 and references therein.
[44] E. J. Corat and D. G. Goodwin, J. Appl. Phys. **74**, 2021 (1993).
[45] C. R. Brazier, R. S. Ram, and P. F. Bernath, J. Mol. Spectrosc. **120**, 381 (1986).
[46] PGOPHER spectral simulation program written by C. M. Western. A summary of the program and the Hamiltonian used is given in M. E. Green and C. M. Western, J. Chem. Phys. **104**, 848 (1996).
[47] P. W. Fairchild, G. P. Smith, D. R. Crosley, and J. B. Jeffries, Chem. Phys. Lett. **107**, 181 (1984).
[48] A. P. Thorne, *Spectrophysics*, 2nd ed. (Chapman and Hall, New York, 1988), Chap. 11.
[49] T. M. Hong, S. H. Chen, Y. S. Chion, and C. F. Chen, Thin Solid Films **270**, 148 (1995).